Isospin forbidden and allowed reactions $^{16}O(\alpha,\alpha_0)^{16}O$ and $^{16}O(\alpha,\gamma)^{20}Ne$

D. J. Steck*
Department of Physics, University of Wisconsin, Madison, Wisconsin 53706
(Received 7 September 1977)

Six ^{20}Ne levels have been investigated in detail via the $^{16}O + \alpha$ channel between $6.9 \leq E_\alpha \leq 10.2$ MeV. Level parameters for states at $E_x(^{20}Ne) = 10.264 \pm 0.008$, 11.077 ± 0.008, 11.259 ± 0.008, 11.552 ± 0.008, 12.237 ± 0.008, and 12.390 ± 0.008 MeV have been extracted from γ decay properties and phase shift analysis of the elastic scattering. With the exception of the 11.552 and 12.39 MeV states, these levels display primarily $T = 1$ characteristics. In addition to some previously reported $T = 0$ states, several other weak γ decaying resonances were observed at 11.97 ± 0.04, 12.05 ± 0.04, and 12.49 ± 0.02 MeV but were not studied in detail. Charge dependent matrix elements (4–120 keV) for isospin mixing of $T = 1$ states with nearby $T = 0$ states were estimated from the measured level parameters.

[NUCLEAR REACTIONS $^{16}O(\alpha,\alpha_0)^{16}O$, $^{16}O(\alpha,\gamma_{0,1,2})^{20}Ne$, $^{16}O(\alpha,\alpha_2\gamma_{6.13})^{16}O$, $E_\alpha = 6.9$–10.2 MeV; measured $\sigma(E,\theta)$. Deduced ^{20}Ne level parameters, J, π, T, γ-branching ratios, Γ_γ, Γ, E_R. Isospin mixing, charge dependent Hamiltonian, IAS.]

I. INTRODUCTION

The role of charge dependent forces in nuclear reactions has been the focus of experimental and theoretical interest for many years. Early observations and calculations[1,2] discovered that the low lying nuclear states in light nuclei possessed high isospin purity. Hence the dominant component of the nuclear interaction in this region can only weakly depend on charge. At higher excitation energies, a high density of $T_<$ ($|T_<| = t_3$) states, which may strongly mix with $T_>$ ($|T_>| = t_3 + 1$) states, weakens the concept of a unique isospin assignment for any physical state and therefore obscures the role of charge dependent forces. Although recent studies[3] may indicate some reestablishment of isospin conservation at higher excitation energies, an extraction of the strength of the charge dependent force is extremely difficult.

In light even-even nuclei, like ^{20}Ne, the first few $T_>$ (= 1) states occur at moderate excitation energies (~10 MeV) where the density of $T_<$ (= 0) levels is low enough to expect that isospin mixing may involve only one $T_>$ and one $T_<$ state. Nuclear reactions between $T = 0$ nuclei, ^{16}O and ^4He, for example, should form only $T = 0$ compound nuclear ^{20}Ne levels in the absence of charge dependent forces. However, small isospin impurities can be introduced through the Coulomb interaction and any charge dependent component of the nuclear interaction. Since only $T = 0$ particle exit channels and the inherently weak γ decay are available to these $T = 1$ ^{20}Ne states below 12.8 MeV, we would expect them to have quite narrow widths and to display a strong $T = 1$ γ decay. Since the extraction of the total charge dependent interaction is simplified for such levels, the primary goal of this study was to obtain the strength of this interaction through a measurement of the level parameters of the low lying, natural parity $T = 1$ states in ^{20}Ne.

Compound nuclear formation via the isospin forbidden elastic scattering (ES) and radiative capture (RC) reactions of ^{16}O and ^4He provide the most sensitive method of obtaining these level parameters with present experimental techniques. The only comprehensive RC survey in this region,[4] $10 \leq E_x(^{20}Ne) \leq 12.8$ MeV, had located several narrow resonances but had studied only two in detail. Although the ES reaction had been studied extensively the most recent survey[5] had insufficient energy resolution (~8 keV) to resolve extremely narrow resonances. Thus the present work sought to improve and extend these measurements by taking a survey of the RC reaction and then studying each resonance in detail with high energy resolution through both reaction channels.

II. EXPERIMENTAL PROCEDURE

This experiment consisted of three stages. The first stage surveyed the RC γ decays to the ground (γ_0), first two excited states (γ_1,γ_2), and first to ground state transition ($\gamma_{1\to 0}$) for incident beam energies from 6.9 to 10.2 MeV. During the second stage, the γ decay properties of each suspected resonance were studied in greater detail. The third stage concentrated on simultaneously measuring multiangle ES excitation functions and the

RC excitation function for the primary γ decay at 90°. During all stages, an α beam, whose homogeneity we believe to be better than 1 keV, from our Pelletron-charged EN tandem Van de Graaff was used to bombard differentially pumped O_2 (99.995% pure) gas targets. Since typical beam currents of He^{++} were limited to 100–700 nA by collimating slits, individual detector counting rates were low enough to use standard slow electronic signal processing. Each detector's spectra were stored in our DDP-124 computer where they could be monitored on line, written on magnetic tape, and later recalled for analysis. Cross sections were calculated from background subtracted peak yields in the following manner. A spectrum was read back from magnetic tape and displayed on a cathode ray tube. Each peak yield was then calculated as the net counts above a computer generated background function which was visually adjusted to match local conditions. This method proved quite adequate for ES spectra that contained isolated peaks superimposed on low backgrounds. However, in order to obtain reproducible peak yields from complex γ-ray spectra, it was necessary to incorporate a least squares local background fitting procedure and an independent peak intensity calculation.[6]

During the first stage of the experiment, a search was conducted at 50 keV intervals for narrow γ decaying resonances. One 50 cm^3 Ge(Li) detector at 0° was placed at 4 cm from the target's end to view a 60–80 keV target thickness [see Fig. 1(a)]. Another 50 cm^3 Ge(Li) detector at 135°, 17.5 cm was added during later runs to increase the sensitivity for $E1$ and $E2$ transitions to the ground state. The development of a compact, differentially pumped gas target chamber[7] and a continuous airflow calorimeter[8] for measuring incident beam flux, allowed clean γ spectra to be obtained for total incident beams of ~1 mC.

An array of two moveable NaI detectors (θ = 75°, 60° and 35°, 25°) and one fixed NaI detector (θ = 90°) were added to the two Ge(Li) detectors' arrangement for the second stage. After each suspected resonance was located, angular distributions were measured both on and off resonance, while the Ge(Li) detectors accumulated detailed spectra. Since only minimal shielding was utilized to mask the beam stop, the NaI detectors were susceptible to pileup from the 6.13 MeV contaminant line of $^{13}C(\alpha,n\gamma)^{16}O$.

Each suspected resonance was investigated further during the third stage by simultaneously measuring the ES excitation functions at 15 angles between $60° \leq \theta_{c.m.} \leq 168°$ and the RC excitation function at 90° in a larger volume scattering chamber.[9] [See Fig. 1(b)]. Narrow slit systems and

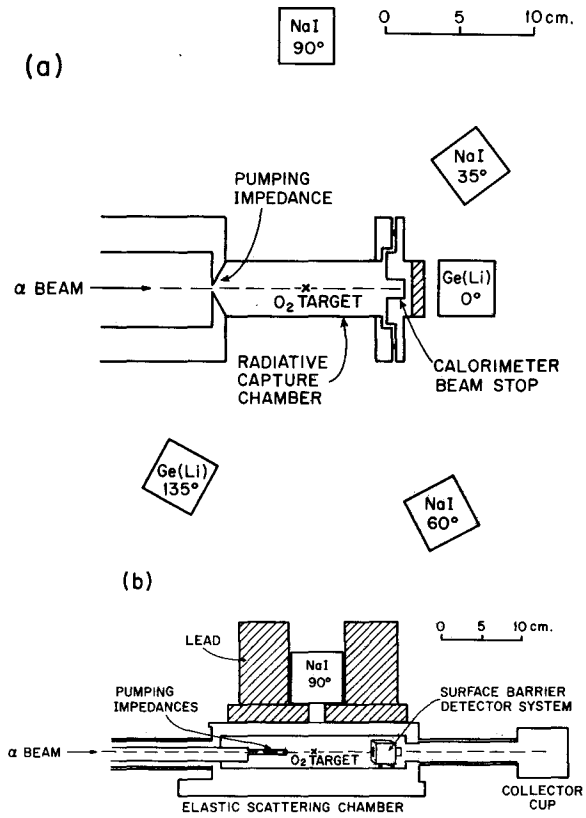

FIG. 1. Experimental arrangements. Part (a) is a schematic (top view) of the γ detectors and the radiative capture chamber (only the two Ge(Li) detectors were present during the preliminary survey). Part (b) shows (side view) the position of the NaI monitor detector relative to one of the surface barrier detectors during the third stage of the experiment.

low (10 Torr) gas pressures limited the target thickness viewed by the surface barrier detectors to 1–3 keV, while lead shielding defined an effective target thickness for the 90° NaI detector to be 10–30 keV and masked the beam stop. To insure that the proper energy region was covered, each resonance was located by monitoring the RC excitation function taken in 5 keV steps and then remeasuring the region using smaller (1 to 2 keV) steps.

Uncertainties in the measured cross sections are typically 3% for the ES reaction and 10 to 15% for the RC reaction. Statistical uncertainties were generally of the same size for peaks from both reactions. The major contribution to the RC uncertainties comes from the absolute γ detection efficiency. Each γ detector's efficiency was measured for each experimental arrangement as follows. For $E_\gamma < 2$ MeV, calibrated sources were inserted at the target position. Having thus established the low energy efficiency, we extended it to

12 MeV by observing cascades from proton radiative capture reactions and the two line method.[10]

III. RESULTS

Figures 2 through 7 show the RC and ES data in limited energy regions around narrow structures seen in the preliminary RC survey ($6.9 \leq E_\alpha \leq 10.2$ MeV). These regions were selected since they showed significant γ-ray yields for either γ_0, γ_1, or γ_2 (along with $\gamma_{1\to 0}$). The lower energy scale in all figures is the laboratory beam energy at the center of the chamber. Excitation energies in ^{20}Ne ($Q = 4.73$ MeV) can be found on the upper energy scale. The absolute uncertainty in these energy scales is ±10 keV.

RC cross section error bars [Figs. 2(a) through 7(a)] reflect statistical uncertainties only. When the cross sections are quoted in relative units they have a 10% relative uncertainty. In these cases, the absolute cross sections correspond to an ordinate scale in units of μb/sr but with a 50% uncertainty. Error bars for ES cross sections are a quadrature sum of statistical and other experimental (2%) uncertainties. The solid curves shown on all figures result from the analysis outlined in Sec. IV.

The present RC results generally agree with the survey of Pearson and Spear.[4] Although only the ES data taken very close to each resonance are shown, a wider energy region was studied. These data generally agree with the results of John, Aldridge, and Davis.[5] A more detailed comparison of the present results with previous works is given in Sec. V.

IV. ANALYSIS

To estimate a level's isospin purity, one needs accurate values for the total and partial decay widths, resonant energy, and spin and parity. Therefore, data from both reactions underwent detailed analysis to fix the most consistent set of resonance parameters. Since we sought those levels that were primarily $T = 1$, the first step must be a tentative isospin identification procedure. Isospin conservation would inhibit the formation of a $T = 1$ state from two $T = 0$ nuclei and further inhibit its subsequent decay into that same channel. Therefore a state that is primarily $T = 1$ should possess an extremely small α width. If such a state is formed in the self-conjugate nucleus ^{20}Ne, isospin selection rules[11] would favor $\Delta T = 1$, electric ($E1$) or magnetic ($M1$) dipole radiative decay. Thus, structures were tentatively identified as $T = 1$ states if they showed both a narrow total width and a strong γ decay to one of the low lying ($T = 0$) levels of ^{20}Ne.

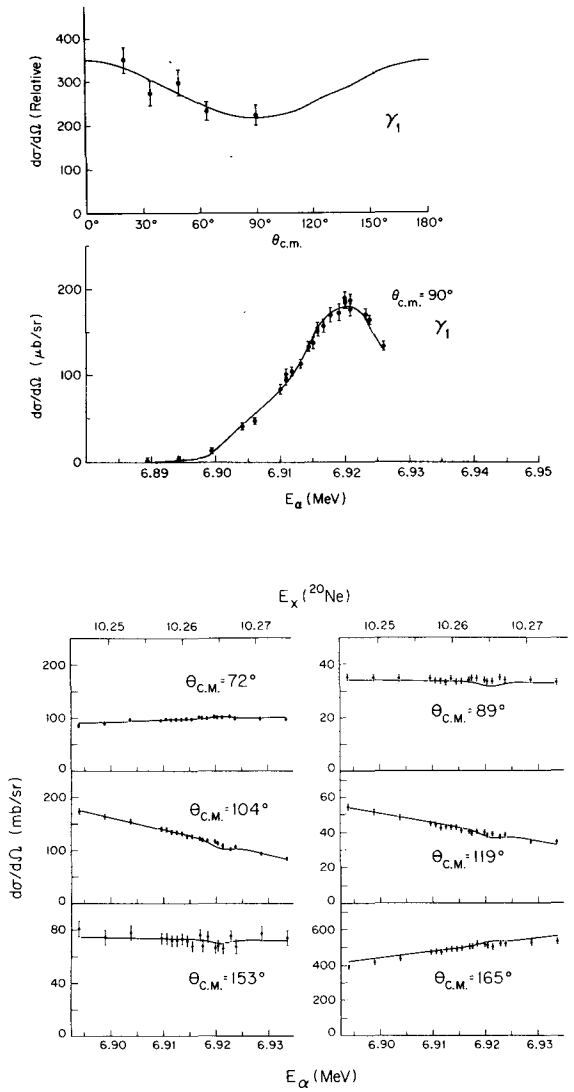

FIG. 2. The $E_\alpha = 6.92$ MeV resonance ($E_x = 10.26$ MeV). Part (a) contains the γ_1 angular distribution (top) and the γ_1 RC excitation function (bottom). The angular distribution is best fit [confidence level (CL) = 0.6] by a $2^+ \to 2^+$, $M1$ transition (solid line). The γ_1 RC excitation function was fitted (solid line CL = 0.4) with a modified thick target form (1) to reproduce the experimentally observed target edge blurring effects caused by shielding penetration and target-to-detector distance variations. Part (b) shows the ES scattering data taken simultaneously with the γ_1 RC excitation function. Excitation functions are shown at 6 (from a total of 15) angles which display the largest resonant structure. The solid line results from a global phase shift fit (see Sec. IV) which includes the contribution from a 300 eV, $L = 2$ resonance. Since the resonant contribution only marginally improves the CL from 0.4 to 0.45, we set an upper limit on the width of 0.3 keV. The error bars shown are a quadrature sum of statistical and other experimental (~2%) errors. The energy scales have been corrected for energy loss to the center of the chamber.

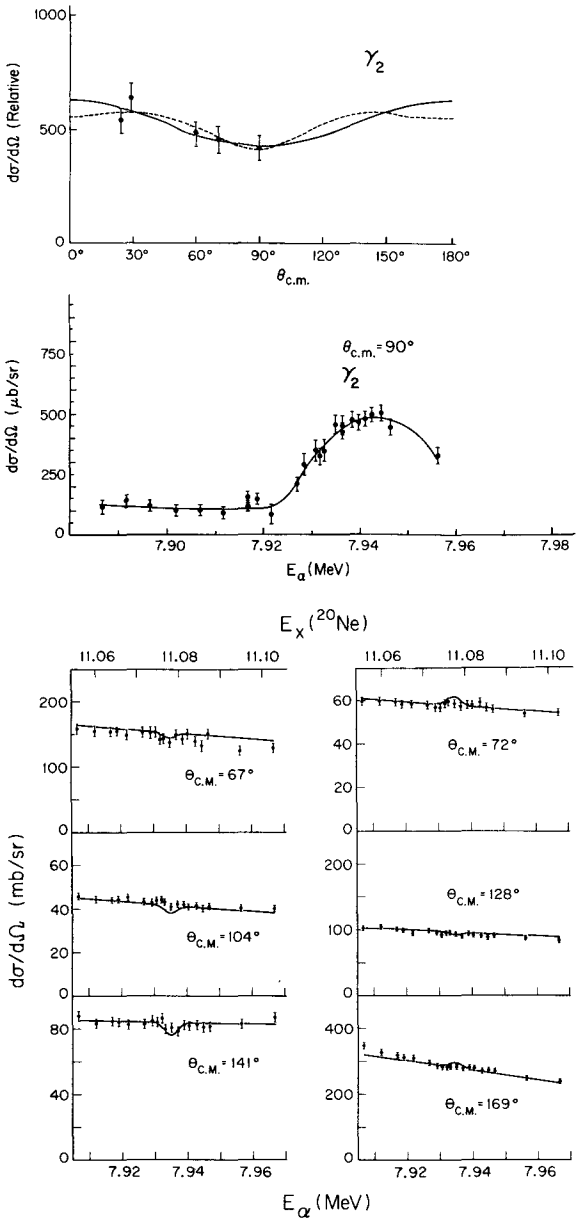

FIG. 3. The $E_\alpha = 7.93$ MeV resonance ($E_x = 11.08$ MeV). Same format as Fig. 2. The γ_2 angular distribution can be fitted by either a dipole (solid line, CL = 0.6) or a quadrupole (dashed line, CL = 0.5) distribution. The thick target fit has a CL = 0.25. The ES fit includes a 500 eV, $L = 4$ resonance.

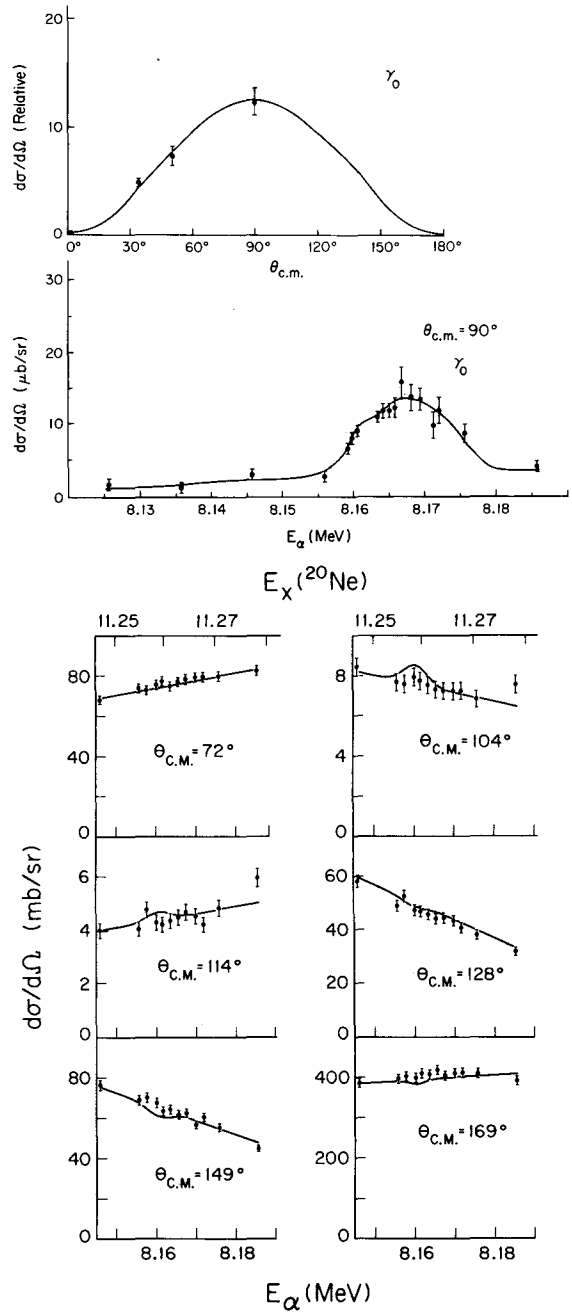

FIG. 4. The $E_\alpha = 8.16$ MeV resonance ($E_x = 11.26$ MeV). Same format as Fig. 2. The angular distribution fit is typical of a $1^- \rightarrow 0^+$, $E1$ transition. The γ_0 excitation function fit has a CL of 0.9. The ES fit includes the contributions from a 300 eV, $L = 1$ resonance.

The RC excitation functions were fitted with a modified isolated resonance yield expression

$$Y(\theta) = Y_0(\theta) + D(E_R) Y_\infty(\theta) \times \left[\tan^{-1}\left(\frac{2(E - E_R)}{\Gamma_T}\right) - \tan^{-1}\left(\frac{2(E - E_R - \rho)}{\Gamma_T}\right)\right] + C(E_R), \quad (1)$$

where E_R is the resonant energy, Γ_T is the full width at half maximum (FWHM), ρ is the target thickness, Y_0 is the off resonant yield, Y_∞ is the thick target yield, and $D(E_R), C(E_R)$ are functions that correct for source to detector distance and shielding penetration variations. The form of

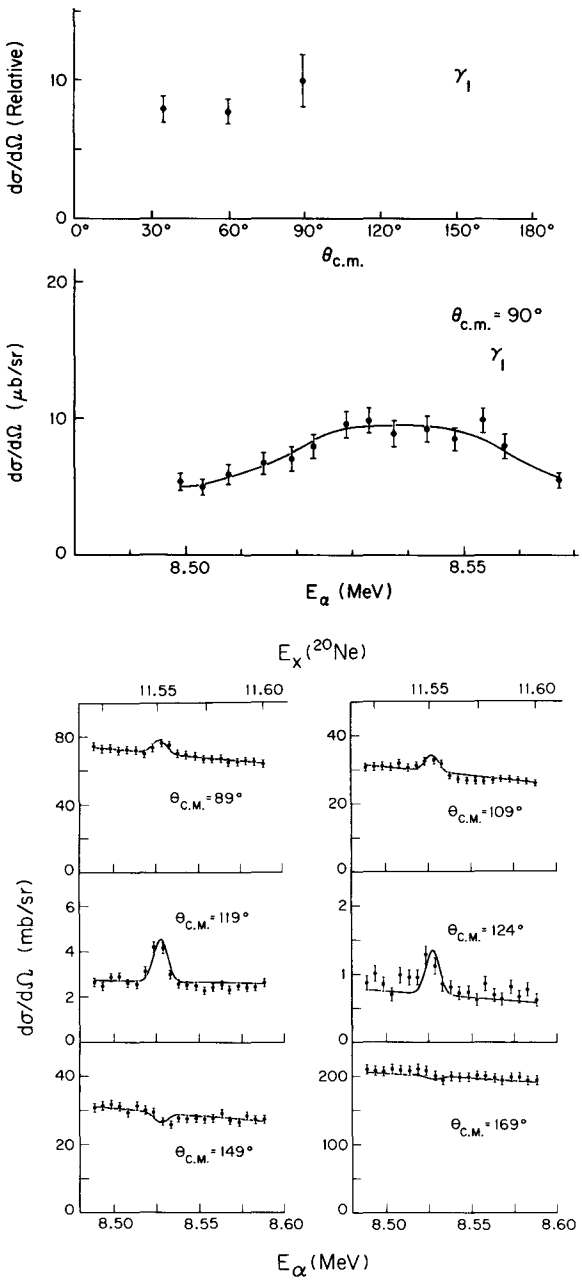

FIG. 5. The $E_\alpha = 8.53$ MeV resonance ($E_x = 11.55$ MeV). Same format as Fig. 2. No fit is shown for the angular distribution since an isotropic fit (CL = 0.2) was as significant as higher orders. The γ_1 excitation function fit (CL = 0.4) shows a definite, albeit weak resonance. The ES excitation function fit includes the contribution from a 900 eV, $L = 2$ resonance.

these functions was determined from separate yield measurements taken in the extended target chamber geometry with a localized source that reproduced the path a narrow resonance would follow as the incident beam energy varied. While

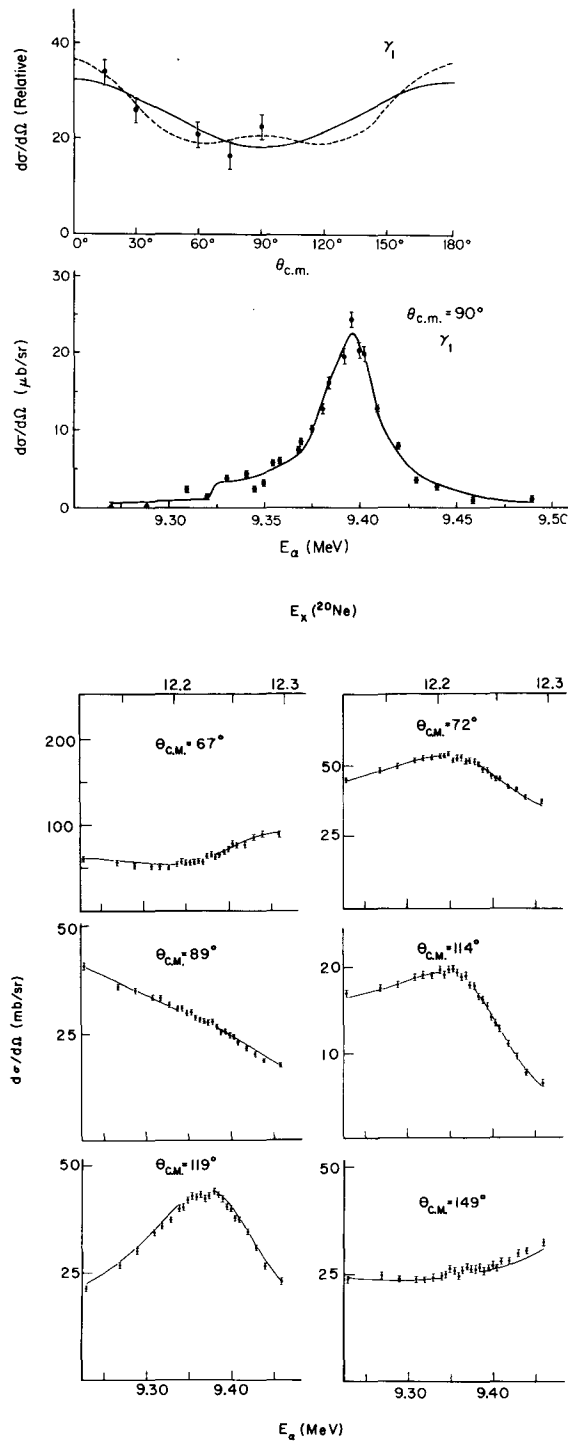

FIG. 6. The $E_\alpha = 9.38$ MeV resonance ($E_x = 12.24$ MeV). Same format as Fig. 2. The γ_1 angular distribution indicates either a dipole (solid line, CL = 0.35) or quadrupole (dashed line, CL = 0.4) transition. The γ_1 excitation function fit (CL = 0.3) is characteristic of our nonthick target yields. The solid line representing the global phase shift fit was omitted from the ES excitation functions in the region of the RC resonance to highlight the small deviations.

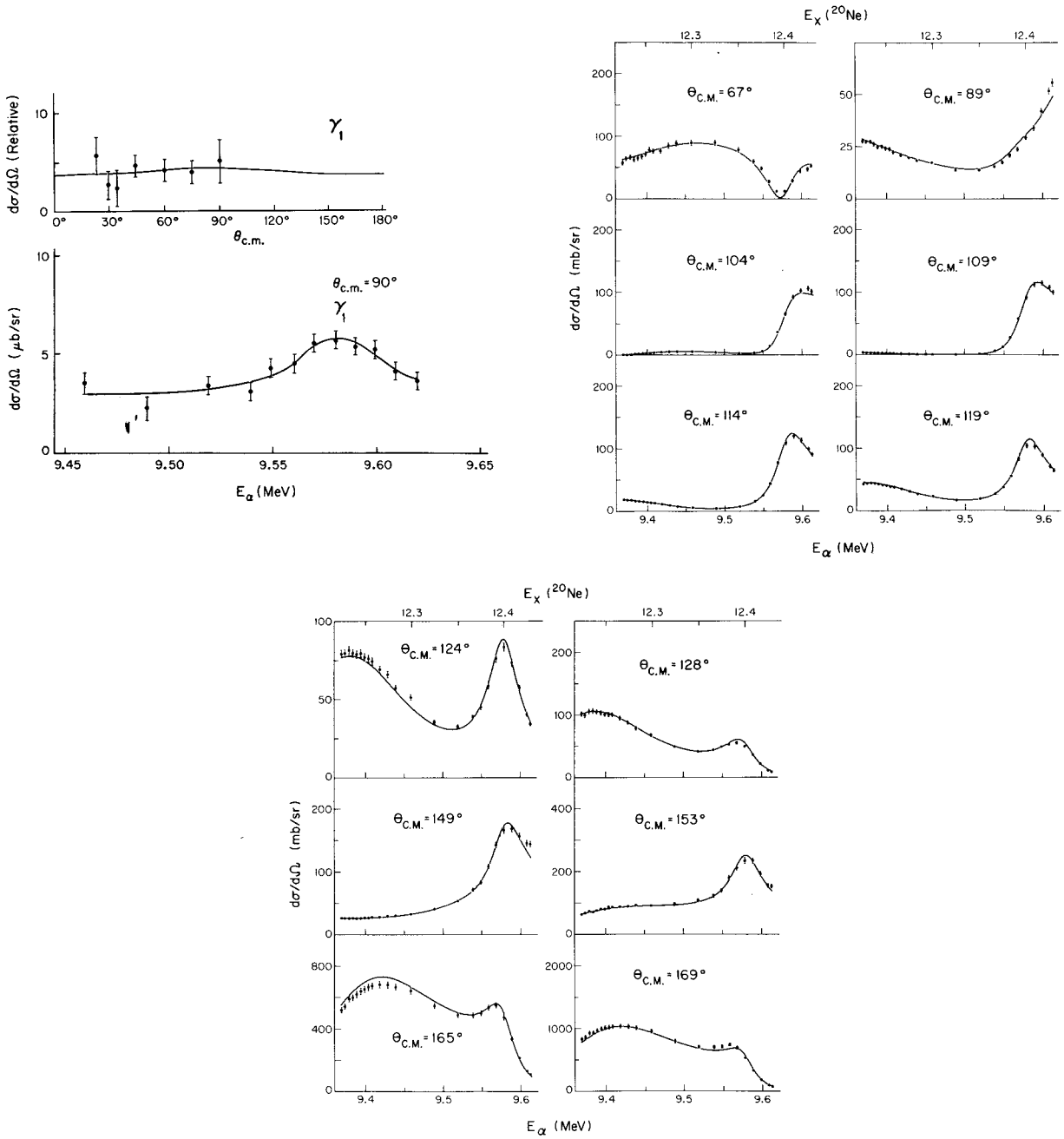

FIG. 7. The E_α =9.57 MeV resonance (E_x =12.39 MeV). Same format as Fig. 2. The γ_1 angular distribution can be described by an isotropic (CL=0.4) or dipole (CL=0.5, solid line) expansion. The γ_1 excitation function has a CL=0.8. The ES, global phase shift fit required a 148 keV wide, 4^+ level at 9.39 MeV and a 33 keV wide, 3^- level at 9.58 MeV.

the fits produced accurate values for E_R and Y_∞, these geometric effects allowed us to set only upper limits on Γ_T.

Since the incoming spin system, $0^+ + 0^+$, can only form natural parity states in the $m=0$ substate, deexcitation γ-ray multipolarities can be determined from a fit of the angular distribution of primary γ decays to the form

$$W(\theta) = \sum_{k=\text{even}}^{4} a_k P_k(\cos\theta)\,, \qquad (2)$$

where P_k is the Legendre polynomial and a_k is the normalized ($a_0=1$) coefficient. The initial state's spin (J) can be implied from a comparison of the corrected (for large angular acceptance) experimental coefficients (b_k) with the theoretical calcu-

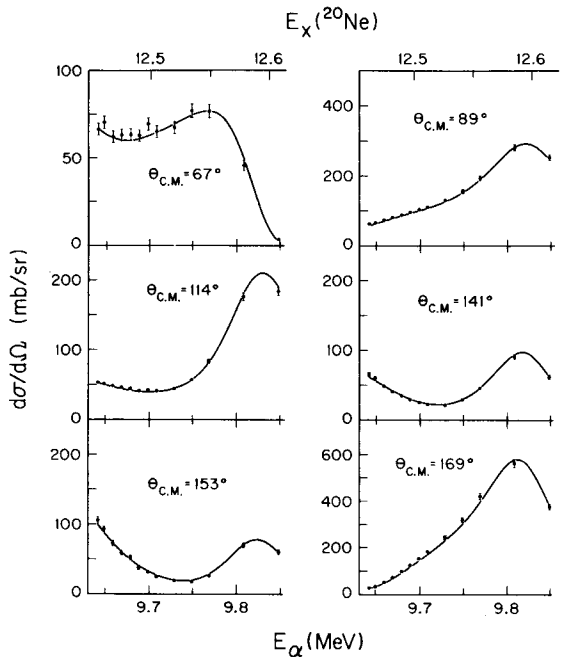

FIG. 8. The $E_\alpha = 9.72$ MeV region ($E_x = 12.49$ MeV). Same format as Fig. 2, part (b). The ES excitation functions were adequately reproduced by a 88 keV wide, 6^+ level at 9.82 MeV.

lations for different multipole transitions to the final state from different initial state J's.[12] The results of these fits and comparisons are listed in Table I. This procedure could not unambiguously determine J for some weak γ transitions.

Transition strengths ($\omega\gamma_i$) were calculated from

$$\omega\gamma_i = \frac{2\eta Y_\infty(\theta)}{\lambda^2 n \epsilon_i N \langle W_i(\theta) I(\theta)\rangle}\left(\frac{M_{^{16}O}}{M_\alpha + M_{^{16}O}}\right), \tag{3}$$

where W, Y_∞ are defined above, η is the target stopping power, ϵ_i is the absolute detection efficiency, λ is the center of mass wavelength, N is the number of target nuclei/cm^3, n is the number of incident α's, and I is the relativistic intensity tranformation to the lab frame. The brackets denote an average of $W(\theta)I(\theta)$ over the detector's angular acceptance. The partial decay with ($\Gamma_{\gamma i}$) can be obtained from $\omega\gamma_i$ (assuming $\Gamma_T \simeq \Gamma_\alpha$)

$$\omega\gamma_i = \Gamma_{\gamma i}\Gamma_\alpha(2J+1)/\Gamma_T\,. \tag{4}$$

The reduced transition strength ($|M|^2 = \Gamma_{\gamma i}/\Gamma_{\text{W.u.}}$) for each decay branch can then be compared with theoretical predictions and previous experimental observations for similar transitions. Transition strengths for secondary branches can be calculated from (3), (4), and the observed yields

TABLE I. Measured angular distribution coefficients.

E_α	Final state J^π; E_x (MeV)	CL[a]	a_2/a_0	a_4/a_0	b_2/b_0[b]	b_4/b_0[b]
6.92	2^+; 1.63	0.6	0.33 ± 0.09	•••	0.38 ± 0.10	•••
		0.2	0.33 ± 0.09	0.03 ± 0.13	0.38 ± 0.10	0.04 ± 0.15 ($\delta = -0.1 \pm 0.2$)[c]
7.93	4^+; 4.25	0.6	0.26 ± 0.10	•••	0.29 ± 0.11	•••
		0.5	0.25 ± 0.10	−0.10 ± 0.2	0.28 ± 0.11	−0.12 ± 0.20 ($\delta = -0.27 \pm 0.30$)[c]
8.16	0^+; 0	0.5	−0.99 ± 0.10	•••	−1.08 ± 0.10	•••
8.53	2^+; 1.63	0.2	•••	•••	•••	•••
		0.25	−0.1 ± 0.20	•••	−0.11 ± 0.3	•••
9.38	2^+; 1.63	0.35	0.39 ± 0.11	•••	0.43 ± 0.12	•••
		0.4	0.34 ± 0.12	0.30 ± 0.20	0.40 ± 0.13	0.35 ± 0.25 ($\delta = -0.1 \pm 0.07$)[c]
9.57	2^+; 1.63	0.4	•••	•••	•••	•••
		0.5	−0.12 ± 0.30	•••	−0.13 ± 0.30	•••
		0.2	−0.11 ± 0.30	0.10 ± 0.40	−0.12 ± 0.30	0.10 ± 0.4
9.70	2^+; 1.63	0.5	•••	•••	•••	•••
		0.5	0.2 ± 0.20	•••	0.2 ± 0.2	•••

[a] CL denotes angular distribution fit confidence level (0.1 to 0.9 acceptable).
[b] Coefficients corrected for angular acceptance and edge effect.
[c] $\delta = \langle E2\rangle/\langle M1\rangle$.

TABLE II. Radiative capture resonance parameters.

E_α (MeV)	E_x (MeV)	$\Gamma^T_{c.m.}$ (keV)	Final state (J^π; E_x)	$\omega\gamma_{c.m.}$ (eV)	Branching ratio	$\Gamma^\gamma_{c.m.}$ [a] (eV)	$\lvert M\rvert^2$ [b] (W.u.)	
6.918±0.01 [c]	10.264	≤1	0^+; 0		≤0.1			
			2^+; 1.63	19.2 ±1.9	1.0	3.85±0.39	0.28	($M1$)
			2^-; 4.97		≤0.2			
			3^-; 5.62		≤0.2			
7.932±0.01	11.077	≤3	0^+; 0		≤0.01			
			2^+; 1.63		≤0.02			
			4^+; 4.25	30.4 ±3	1.0	3.4 ±0.3	0.50	($M1$)
8.161±0.01	11.26	≤3	0^+; 0	0.58±0.05	1.0	0.19±0.02	2.8×10^{-4}	($E1$)
			2^+; 1.63		0.4±0.1			
8.53 ±0.01	11.55	≤5	0^+; 0		≤0.4			
			2^+; 1.63	0.41±0.05	1.0	0.08±0.01 ($J=2$)	3.9×10^{-3} [0.31	($M1$) ($E2$)]
			4^+; 4.25		0.5±0.4			
			2^-; 4.97		≤0.3			
9.384±0.01	12.237		0^+; 0		0.45±0.10			
		18±5	2^+; 1.63	5.8 ±0.5	1.0	1.2 ±0.1	0.046	($M1$)
			4^+; 4.25		≤0.3			
			2^-; 4.97		≤0.3			
9.57 ±0.01	12.39		0^+; 0		0.01			
		27±5	2^+; 1.63		0.4±0.1			
			4^+; 4.25	1.94±0.15	1.0	0.28±0.02	1.1×10^{-3}	($E1$)
		40±10	$\alpha_2\gamma_{6.13}$	1.96±0.1 [d] $\times10^3$	2.2±0.3 $\times10^3$			
9.70 ±0.03	12.49	≤10	2^+; 1.63	0.17±0.05	1.0			

[a] Assume $\Gamma_\alpha \simeq \Gamma_T$.
[b] Multipolarity based on most likely transition.
[c] The energy uncertainty reflects the maximum of the relative uncertainty and the absolute uncertainty (0.01).
[d] $\omega\gamma = (2J+1)\,\Gamma_\alpha\Gamma_{\alpha_2}/\Gamma$.

$$R_{ij} = Y_i(\theta)\epsilon_j A_j(\theta)/Y_j(\theta)\epsilon_i A_i(\theta) = \Gamma_{\gamma_i}/\Gamma_{\gamma j}\,, \qquad (5)$$

where i and j label the primary and secondary branches, respectively, $A = \langle WI\rangle$, and R_{ij} is the branching ratio. These reduced strengths provide further information to help identify the initial state's spin. A summary of the RC results can be found in Tables I and II.

Some level parameters can also be extracted through a phase shift analysis of the elastic scattering near a resonance. The differential cross section for the simple spin system, $0^+ + 0^+ \to 0^+ + 0^+$ can be expressed as

$$\frac{d\sigma}{d\Omega_{c.m.}}(\theta,E) = \lambda\bar{}^2 \Big| {}^{-\frac{1}{2}}\eta \csc^{2\frac{1}{2}}\theta \exp(i\eta \ln \csc^2\tfrac{1}{2}\theta) + \sum_{l=0}^{L}(2l+1)\exp[i(\alpha_l+\delta_l)] \times \sin\delta_l P_l(\cos\theta)\Big|^2, \qquad (6)$$

where $\lambda\bar{}$ is the center of mass wavelength, η ($= Ze^2/\hbar v$) is the Sommerfeld parameter, α_l is the relative Coulomb phase shift and δ_l is the total nuclear phase shift. The energy dependence of δ_l can be parametrized in terms of resonant (Γ_l, E_R^l) and nonresonant (a_l, b_l) values

$$\delta_l(E) = a_l + b_l\Delta E + \tan^{-1}\left(\frac{\Gamma_l}{2(E_R^l - E)}\right). \qquad (7)$$

Although the partial wave expansion should include an infinite sum of terms, truncation at $L=6$ proved adequate to fit all angular distributions below $E = 9.9$ MeV. Further, we found empirically that real phase shifts were sufficient to fit all data below $E = 9.5$ MeV. A three step process was developed to find the set of parameters for each l that reproduced the ES cross section in the energy region surrounding each suspected $T=1$ resonance. Since even off-resonance phase shifts may contain significant contributions from resonances distant by many half-widths, model predictions (such as the hard core or optical mode) fail to reproduce the observed cross sections even far from sharp resonances (see Fig. 9).

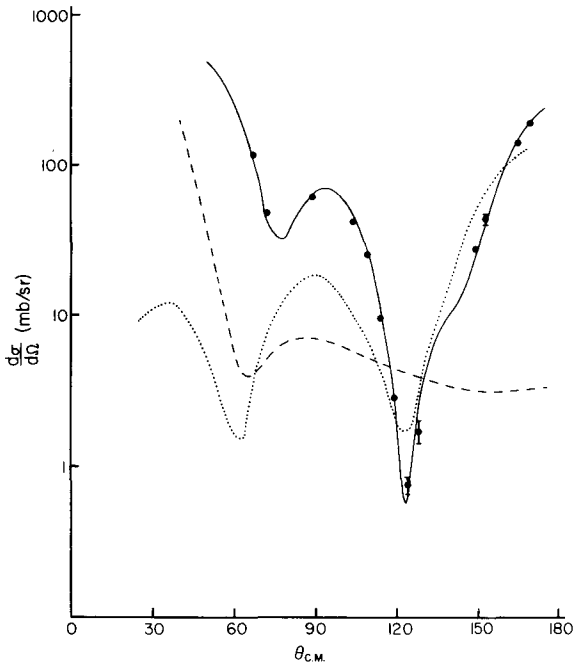

FIG. 9. Typical elastic scattering angular distribution fits. The solid line shows a phase shift analysis fitted ($\chi^2=1.1$) to the angular distribution at $E_\alpha=8.62$ MeV. This energy was selected for comparison since there are no nearby broad resonances to influence the angular distribution. The dashed line represents the hard core model prediction while the dotted line represents an optical model fit.

Therefore, the first analysis step sought to locate all sets of phase shifts ($|\delta_i\rangle$) that fit the angular distribution at the lowest incident energy in the region. These sets were located by a computer program that searched the χ^2 space along each phase shift axis from 0 to π for local minima in χ_j^2

$$\chi_j^2=\frac{1}{N}\sum_{i=1}^{N}\left(\frac{\sigma_M(\theta_i,E_j)-\sigma_c(\theta_i,E_j)}{\Delta\sigma_M(\theta_i E_j)}\right)^2, \tag{8}$$

where the indices i,j label the angle and energy respectively, N is the total number of angles at E_j, σ_M and $\Delta\sigma_M$ are the measured differential cross section and its uncertainty, and σ_C is the calculated cross section from (6). Investigations of typical χ^2 spaces revealed that within each broad minimum (FWHM~30°), there could be several sharp minima (FWHM~2°). Therefore, following the crude grid search ($\Delta\delta_i=18°$), a modified gradient search was conducted around each broad minimum's central grid point and the $2L_{max}+2$ intersections of the phase shift axes with the $L_{max}+1$ dimensional sphere (radius = 18°) centered on the grid point. The variable metric algorithm of Davidon, Fletcher and Powell,[13] (DFP) with cubic interpolation along the local geodesic provided a technique for quickly and accurately obtaining these refined sets of phase shift solutions.

At any single energy, several phase shift sets may adequately fit the angular distribution. However, cross section variations arising from energy dependent resonant, nonresonant or Coulomb interference should be reproduced by a single set of phase shifts. To identify the physical solution, the ability of each phase shift set to fit the energy variation of the excitation function was tested by allowing each phase shift within the set to vary independently at each successive energy. This second step in the analysis procedure was started at the energy searched in the first step and allowed the DFP technique to track with energy both broad and narrow resonance structure. To insure completeness, steps 1 and 2 were repeated starting from the highest energy in the excitation function.

After the second step, from two to four ambiguous solutions ($\langle\chi^2\rangle\leq 3$) often remained. These ambiguities are not physical since we inserted extra degrees of freedom by allowing phase shifts at successive energies to be independent of the phase shifts at the previous energy. Therefore, the final analysis step removed these degrees of freedom by parametrizing the phase shifts as given in (7). The DFP technique was used to minimize the total χ^2 ($=\sum_j\chi_j^2$) over all energies and angles simultaneously. Initial values for the resonant and nonresonant parameters were obtained from the step 2 solutions and, in some cases, a graphical analysis of the excitation functions.[14] In certain energy regions, it was necessary to modify (7) to reproduce local conditions. When the resonant width is much less than the experimental energy resolution, the observed cross section near the resonance results from the integration of the resonance shape (7) folded with the beam's energy distribution. This process destroys both phase and amplitude information in the resonance region. Resonance parameters can be extracted by an iterative process of folding test resonance shapes with the calculated energy distribution and comparing the result with the observed cross section. The total width (1–5 keV) of the experimental energy distribution was estimated from target thickness (0.5–4 keV), Doppler broadening (0.5 keV), and energy spread of the beam (≤1 keV). In extreme cases this procedure can yield only an upper limit on the level's width. Above $E=9.5$ MeV, it was necessary to add a small imaginary component to the $L=3$ phase shift. Although the inelastic channels, α_1 and α_2, were not explicitly measured, Fig. 10 shows that the cross section for $^{16}O-(\alpha,\alpha_2\gamma_{6.13})^{16}O$ is low except for the structure at $E=9.58$ MeV.

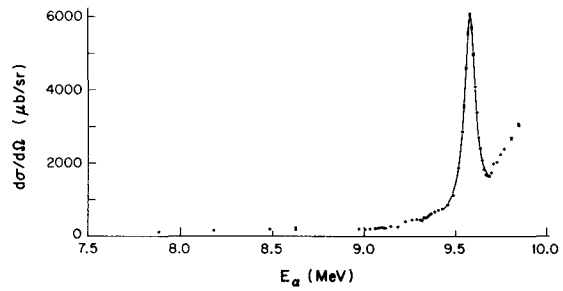

FIG. 10. $^{16}O(\alpha, \alpha_2\gamma_{6.13})^{16}O$ excitation function. Although the inelastic channel ($\alpha_2\gamma_{6.13}$) becomes energetically allowed at $E_\alpha = 7.7$ MeV, the $\gamma_{6.13}$ cross sections are small below 9.5 MeV. A fit (CL = 0.2) to the resonant structure, shown as the solid line, obtained resonance parameters of $\Gamma = 40$ keV at $E_\alpha = 9.57$ MeV. The energy scale has been corrected to the center of the chamber. Only statistical errors are shown.

Since the analysis process is quite complex, each step was tested with computer simulated data sets. In all test cases the procedure unambiguously located the correct parameter set. When the experimental data were analyzed, only one solution emerged from the three step process except near $E = 8.53$ MeV. At this energy, two solutions that differed mainly in the $L = 0$ and $L = 2$ resonant and nonresonant phase shift parameters adequately reproduced the observed cross section. Phase shift parameters are listed in Tables III and IV. The cross sections generated by these values are shown as the solid lines in Figs. 2(b) to 7(b) and 8.

V. DISCUSSION

Several resonance characteristics may be used to establish the identity of the primary isospin component of a state. Although a narrow total decay width may suggest inhibition from isospin conservation, the most convincing evidence for a $T = 1$ assignment results from the selection rules governing dipole radiative decay. Since both $E1$ and $M1$, $\Delta T = 1$ transitions are greatly enhanced over their $\Delta T = 0$ counterparts in a self-conjugate nucleus,[11] the primary criteria used to assign $T = 1$ were the observation of a narrow total width and the presence of a strong dipole decay to a $T = 0$ final state. Supporting evidence for such an assignment also comes from the existence of a properly corresponding state in ^{20}F. Often some of the characteristics of these ^{20}Ne states have been measured by isospin allowed direct reactions. All evidence from the present study and other works used to establish the isospin identity is outlined individually below, under the headings of the resonant incident beam energy (the corresponding ^{20}Ne excitation energy).

1. $E_\alpha = 6.92$ MeV resonance ($E_x = 10.26$ MeV) (see Fig. 2)

A prominent resonance in the decay to both the first excited state (γ_1) and the decay of the first excited state to the ground state ($\gamma_{1\to 0}$) occurs near $E_\alpha = 6.92$ MeV. The measured angular distribution coefficients are most consistent with a $2^+ \to 2^+$, $M1$ transition. The γ_1 transition strength,

TABLE III. Nonresonant phase shift parameters. The nonresonant parameters a_L and b_L from Eq. (7) are given in units of rad and rad/MeV, respectively.

Paramters	E_α (MeV) \ L	0	1	2	3	4	5	6
a_L	6.9	1.95	2.96	2.52	0.20	0.26	1.84	3.13
b_L		−4.2	−5.7	−6.1	0.5	1.2	4.6	0.3
a_L	7.9	1.41	2.90	3.09	2.69	1.58	3.16	0.01
b_L		−0.1	2.5	1.2	−0.5	0.4	0.5	0.3
a_L	8.2	0.31	0.86	2.46	2.84	2.32	3.03	0.02
b_L		1.3	9.6	5.9	0.5	1.5	0.8	0.5
a_L	8.5	0.58	2.24	2.13	2.92	2.57	3.06	0.04
b_L		−0.2	0.2	0.4	−0.2	0.2	−0.3	−0.1
a_L	9.0	0.79	2.57	2.0	3.05	2.70	0.03	0.13
b_L		−0.9	−1.0	1.2	−0.3	−1.1	−1.0	−0.5
a_L	9.4	0.72	2.44	2.83	3.02	2.80	3.12	0.13
b_L		0.8	1.2	−0.7	0.24	1.5	0.1	0.4
a_L	9.8	0.72	2.87	2.9	3.14	0.28	0.24	1.45
b_L		1.5	1.3	4.4	0.7	3.8	1.5	0.7

TABLE IV. Elastic scattering resonance parameters.

E_α (MeV)	E_x (MeV) [a]	J^π	$\Gamma_{c.m.}$ (keV)	γ^2 (keV) [b]	θ^2 (%) [c]
6.92 ±0.01 [d]	10.26	(2^+)	≤0.3	≤0.008	$\leq 1.3\times10^{-3}$
7.93 ±0.01 [d]	11.08	(4^+)	≤0.5	≤0.3	≤0.05
8.16 ±0.01 [d]	11.26	(1^-)	≤0.3	≤0.05	≤0.009
8.24 ±0.01	11.32	2^+	40±10	8.3	1.4
8.528±0.01	11.55	(2^+)	0.9±0.5	0.16	0.03
		(0^+)	1.1±0.5	0.14	0.02
9.043±0.01	11.96	1^-	30±5	4.3	0.72
9.37 ±0.02 [e]	12.23	(2^+)	≤20	<3	≤0.5
9.39 ±0.03	12.24	4^+	148±20	45.7	7.7
9.5 ±0.2	12.3	2^+	~500	~78	~13
9.58 ±0.01	12.39	3^-	37±5	7.5	1.2
9.82 ±0.03	12.59	6^+	88±10	165.4	27.9

[a] Q=4.73 MeV.
[b] $\gamma_L^2 = \frac{1}{2}\Gamma P_L$.
[c] $\theta^2 = 2\mu R^2/3\hbar^2\gamma_L^2\times100$; R=1.4 $(16^{1/3}+4^{1/3})$ fm.
[d] Resonant energy and spin were taken from radiative capture data to extract upper imits on widths from comparative smoothed calculations.
[e] Estimated from graphical analysis.

$\omega\gamma = 19.2\pm1.9$ eV, represents 0.28 Weisskopf unit (W.u.) which strongly suggests $\Delta T = 1$ transition. Generally our measured decay properties agree with the earlier work (Ref. 4) once their radiative strength has been corrected to the center of mass value. Although their result (corrected to the center of mass), $\omega\gamma = 22.4\pm2.4$ eV, is somewhat larger than ours, this may just reflect the difference between the use of background subtracted peak yields of the present work compared with the total window summing technique of Ref. 4. A recent measurement[15] of this radiative strength obtained $\omega\gamma = 19.7\pm1.6$ eV, in accord with the present study. Since this transition is the analog to the Gamow-Teller β decay of ^{20}F, the radiative strength can be compared with the observed and predicted β-decay shape factors (a). Using the present value for $\Gamma_\gamma(M1) = 3.85\pm0.4$ eV, we obtain $a = 0.49\pm0.05$ $(\%/m_0c^2)$ which agrees with the observed, $a = 0.40\pm0.22$ $(\%/m_0c^2)$, and conserved vector current (CVC) predicted, $a = 0.41$ $(\%/m_0c^2)$, shape factors.[16] A fit to the RC excitation function established the resonant energy as $E_\alpha^R = 6.92\pm0.01$ MeV but could only set an upper limit of 1 keV on the total width.

The ES excitation functions taken simultaneously show no resonance structure whose width is larger than 1 keV. To determine an upper limit for the width, computer calculated excitation functions, generated with sample widths for an $L=2$ resonance, were compared with the observed cross sections. The calculations employed the integration-folding procedure outlined in Sec. IV. Sample widths were tried in decreasing size until the decrease in χ^2 was no longer statistically significant. This process set an upper limit of 300 eV for Γ_α. We can compare this result with a calculation for Γ_α based on the measured radiative width and the observed[15,17] ratio of β-delayed α decays to γ_1 decays from this state, $\Gamma_{\gamma1}/\Gamma_\alpha = (3.0\pm0.6)\times10^{-2}$ Our calculated result, $\Gamma_\alpha = 128\pm26$ eV, which represents only 0.02% of the single particle strength, is within the upper bound set by the ES procedure and agrees with the results of Ref. 15, $\Gamma_\alpha = 116\pm20$ eV. Supporting evidence for a $J^\pi;T$ assignment of $2^+;1$ can be found in the results of isospin allowed reactions,[18-21] the prediction that the first $T=1$ ^{20}Ne state will be near 10.22 MeV,[22] and the 2^+ assignment[23] to the corresponding ground states of ^{20}F and ^{20}Na.

2. *E_a = 7.93 MeV resonance (E_x = 11.08 MeV) (see Fig. 3)*

A strong resonance, $\omega\gamma = 30.4\pm3$ eV is present in both the γ_2 and $\gamma_{1\to0}$ survey excitation functions near 7.93 MeV. The measured angular distribution favors a $4^+\to4^+$, $M1$ decay with a small $E2$ admixture ($\delta = 0.3\pm0.3$) or possibly a pure $E2$ $2^+\to4^+$, $6^+\to4^+$ transition. While the reduced matrix element for the $M1$ decay ($|M|^2 = 0.5$) is typical for a $\Delta T=1$ transition in light nuclei, the reduced matrix element for the $E2$ transition ($|M|^2 \approx 156$) is unusually large.[24] Since only a weak branch may be present to the first excited state (2^+) and the more precise results from Ref. 4 excluded the 6^+ possibility, we conclude that the J^π is 4^+. Our strength ($\omega\gamma = 30.4\pm3$ eV) is lower than the 37 ± 4 eV observed by Ref. 4. This difference may result from our improved discrimination against pileup pulses from the contaminant 6.13

MeV γ ray. A fit to the RC excitation function established a resonance energy of 7.93 ± 0.01 MeV and set an upper limit of 3 keV on the width.

Since the ES excitation functions showed no broad ($1 \leq \Gamma \leq 10$ keV) structure in the region of the RC resonance energy, we estimated from computer calculated sensitivities (described above) that the upper limit for the width is 500 eV for an $L = 4$ resonance (700 eV for $L = 2$). Although the $L = 4$ calculation, shown as the solid line in Fig. 4(b), reproduced the weak angular resonance pattern better than an $L = 2$ calculation, the improvement in χ^2 was insufficient to exclude the possibility of an $L = 2$ resonance. Some evidence,[20,19] based on stripping strengths, suggests that a high spin state ($J > 2$) was observed near this energy by the isospin allowed reactions ^{19}F(^{3}He, d)^{20}Ne and ^{21}Ne(d, t)^{20}Ne. The absence[25] of a strong γ decaying level at this energy from the reaction ^{12}C(^{12}C, $\alpha\gamma$)^{20}Ne coupled with a 4^+ assignment[26] of the ^{20}F state at 0.823 MeV supports our 4^+; 1 assignment for the ^{20}Ne level at 11.08 MeV.

3. E_a = 8.16 MeV resonance (E_x = 11.26 MeV) (see Fig. 4)

The RC survey excitation functions display a weak resonance near 8.16 MeV for both γ_0, $\omega\gamma_0 = 0.58 \pm 0.05$ eV and γ_1, $\omega\gamma_1 = 0.23 \pm 0.02$ eV. The measured angular distribution coefficients establish the γ_0 decay as a $1^- \rightarrow 0^+$, $E1$ transition. Although the decay strength is somewhat weaker than the average allowed ($\Delta T = 1$) $E1$ transitions ($\omega\gamma \sim 5$ eV), other examples of similar weak allowed transitions have been observed.[11] In fact, as Ref. 11 points out, allowed $E1$ transitions can be inhibited for a variety of reasons while forbidden strengths may be enhanced. Thus, the observed transition strength does not definitively establish nor exclude a $\Delta T = 1$ transition. A fit to the RC excitation function established a resonant α energy of 8.16 ± 0.01 MeV and set an upper limit of 3 keV on the width.

The gross structure of the ES near 8.2 MeV is dominated by a 172 keV, 1^- state at $E_x = 11.23$ MeV and a 53 keV, 2^+ state at 11.33 MeV.[5] Since the off-resonant cross section is lower at some key angles, we estimate our sensitivity to be 300 eV for a 1^- state. Some evidence exists for a 1^-; 1 ^{20}Ne level near this energy from an isospin allowed reaction.[19] However, more convincing supporting evidence for our assignment comes from a recent determination of $J^\pi = 1^-$ for the ^{20}F level at 0.984 MeV.[19,26] Thus the combined evidence from the RC, ES, isospin allowed reactions, and analog identification all favor a 1^-; 1 assignment for the 11.26 MeV state of ^{20}Ne.

4. E_a = 8.53 MeV resonance (E_x = 11.55 MeV) (see Fig. 5)

A weak resonance, primarily γ_1 ($\omega\gamma_1 = 0.41 \pm 0.05$ eV), occurs near 8.53 MeV. The observed branching ratios (see Table II) limit spin possibilities to 0^+, 1^-, 2^+, 3^-, or 4^+ and slightly favor a 2^+ assignment. The measured angular distribution suffered from such large errors that an isotropic fit was as significant as higher orders. If we assume $J = 2$ for this state, then the γ_1 transition strength would represent 3.9×10^{-3} W.u. for a pure $M1$ decay and 0.31 W.u. for a pure $E2$ decay. These reduced matrix elements imply either an inhibited $\Delta T = 1$ or an enhanced $\Delta T = 0$ transition. A fit to the RC excitation function obtained a resonance energy of 8.53 ± 0.01 MeV and set an upper limit of 5 keV on the total width.

The ES excitation functions display a narrow resonance at 8.528 MeV. While the resonant angular distribution is most typical of an $L = 2$ level, the modified global phase shift fit found two acceptable solutions [fit confidence level (CL) between 0.1 and 0.9]. Both an $L = 2$ (CL = 0.1) and $L = 0$ (CL = 0.3) reproduced the observed resonance behavior when coupled with different sets of off-resonant phase shifts. This ambiguity results from the removal of both phase and amplitude resonant interference through the integration-folding process present when using inadequate experimental energy resolution. Both solutions required approximately the same resonance energy (8.528) and width (1 ± 0.5 keV).

Although a number of ^{20}Ne levels have been reported near this energy, the observed characteristics often conflict so we present a brief comparison of those levels to our 11.55 MeV state. The $E_x = 11.53$ MeV member of the doublet observed[27] in the ^{12}C(^{12}C, $\alpha\gamma$)^{20}Ne reaction has been identified as having unnatural parity (3^+, 4^-) on the basis of falling cross section near 0° for one bombarding energy. Since we can only observe natural parity states and since this level decays mainly to the 4.97 MeV state rather than the 1.63 MeV state, this is not the same level as we observe at $E_x = 11.55$ MeV. The 11.56 MeV member has also been tentatively identified[27] as having unnatural parity, but it appears to decay strongly to the 1.63 MeV state. The branching ratios of the 11.59 ± 0.03 MeV state reported[28] in ^{19}F(^{3}He, $d\gamma$)^{20}Ne agree with our results, but they report an $\sim 10^4$ larger Γ_γ/Γ ratio than we see. If their Γ_γ/Γ ratio is correct, one needs apparently three closely spaced γ decaying states, around 11.56 ± 0.03 MeV. Some evidence[18,19,29] exists for a state with $T = 1$ character in this region. However, these studies assigned no firm spin and parity.

Information about possible states in ^{20}F(~1.3

MeV) has also been conflicting. A series of experiments has assigned a spin and parity of 2^- to the level at 1.31 MeV.[26,30] This ^{20}F state, which is weakly populated in stripping reactions, has also been observed[31] with ^{14}N(^{7}Li,p)^{20}F, a reaction that probably is compound nuclear in nature. The spectrum (Fig. 1, Ref. 31) appears to have more than one structure at 1.31 MeV about which the authors, unfortunately, do not comment. Thus the combined evidence for the $E_x = 11.55$ MeV ^{20}Ne state selects $J = 0^+$ or 2^+ while T can be either 0 or 1.

5. $E_\alpha = 9.38$ MeV resonance ($E_x = 12.24$ MeV) (see Fig. 6)

A moderately strong, relatively broad resonance occurs near 9.4 MeV in both the γ_1, $\omega\gamma = 5.8 \pm 0.5$ eV and γ_0 RC survey excitation functions. The γ_1 measured angular distribution coefficients are consistent with a $2^+ \rightarrow 2^+$, $M1$ transition with a possibility of a small ($\delta = 0.1 \pm 0.07$) $E2$ admixture. The radiative width $\Gamma_\gamma = 1.2 \pm 0.1$ eV(0.046 W.u.) is sufficiently large to establish $\Delta T = 1$ radiation character. A fit to the RC excitation function obtained a resonant energy of 9.38 ± 0.01 MeV and a total width of 18 ± 5 keV. The RC results generally agree with, but improve upon, the limited measurements reported in Ref. 4. However, a new, solid target measurement[28] of the radiative capture in this region indicates that this level is a doublet composed of a narrow ($\Gamma < 2$ keV), $J^\pi = 2^+$ resonance at 9.359 ± 0.005 MeV and a broader ($\Gamma \simeq 5$ keV), $J^\pi = 2^+, 3^-$ resonance at 9.407 ± 0.006 MeV. While our RC data are compatible with these results, the extended nature of our gas target led to off-resonance γ-penetration of our shielding and prevented the resolution of such a doublet. Although we observe a larger γ_0 branching ratio, our γ_1 strength ($\omega\gamma_1 = 5.8 \pm 0.5$ eV) agrees with the 5.36 $\pm$ 1.02 eV summed strengths of Ref. 28, and our angular distribution coefficients are consistent with their measurements of the 9.359 MeV resonance.

Above 9 MeV the ES excitation functions display several broad $T = 0$ states (see Table V and also Ref. 5). Between $9.2 \leq E_\alpha \leq 9.5$, our data required resonances at 9.39 MeV ($J^\pi = 4^+$, $\Gamma = 148$ keV) and 9.5 MeV ($J^\pi = 2^+$, $\Gamma = 500$ keV) to reproduce the observed broad structure. However, in the vicinity of the γ decaying resonance some weak fine structure was not reproduced by these two levels. A global phase shift fit, modified to include interference between the 500 keV wide level and a narrow γ decaying level was unable to determine unambiguously the narrow level's parameters. To help display this fine structure, the solid line in Fig. 6(b), is omitted in that region. Our ES evidence does not support the reported[28] upper member of the doublet as an isolated $\Gamma = 5$ keV 3^- level at 9.407 MeV. Although both the α_1 (0^+) and α_2 (3^-) inelastic channels are open, we do not observe any strong resonant structure in the $\alpha_2\,\gamma_{6.13}$ excitation function (see Fig. 10) at this energy. Therefore we conclude that this upper member of the doublet either has a total width smaller than 2 keV, has $J^\pi = 2^+$, or has a large α_1 partial width. A γ decaying level near 12.2 MeV in ^{20}Ne has also been reported[28,32] from the reactions ^{19}F(^{3}He,$d\gamma$)

TABLE V. ^{20}Ne level parameters (summary).

E_α (MeV $\pm$ keV)	E_x(^{20}Ne) (MeV $\pm$ keV)	J^π; T	$\Gamma^T_{c.m.}$ (keV)	$\omega\gamma$ [a] (eV)	$\Gamma_{\gamma i}$ (eV)
6.918 ± 10	10.264 ± 8	2^+; 1	0.13 ± 0.03	γ_1: 19.2 ± 1.9	3.85 ± 0.4
7.932 ± 10	11.077 ± 8	4^+; 1	≤ 0.5	γ_2: 30.4 ± 3	3.4 ± 0.3
8.161 ± 10	11.259 ± 8	1^-; 1	≤ 0.3	γ_0: 0.58 ± 0.05	0.19 ± 0.02
8.24 ± 10	11.32 ± 8	2^+; 0	40 ± 10		
8.527 ± 10	11.552 ± 8	(2^+, 0^+)	1 ± 0.5	γ_1: 0.41 ± 0.05	(0.08 ± 0.01)
9.04 ± 10	11.96 ± 8	1^-; 0	30 ± 5		
(9.05 ± 50)	(11.97 ± 40)		< 40	b	
(9.15 ± 50)	(12.05 ± 40)		< 40	b	
9.384 ± 10 [c]	12.237 ± 8 [c]	2^+; 1 [c]	18 ± 5 [c]	γ_1: 5.8 ± 0.5 [c]	1.2 ± 0.1 [c]
9.39 ± 30	12.24 ± 24	4^+; 0	148 ± 20		
9.5 ± 200	12.3 ± 160	2^+; 0	~500		
9.575 ± 10	12.39 ± 8	3^-; (1)	33 ± 4	γ_2: 1.94 ± 0.15	0.28 ± 0.02
9.60 ± 10	12.41 ± 8	(0^+)			
9.70 ± 30	12.49 ± 24			γ_1: 0.17 ± 0.05	
9.82 ± 30	12.59 ± 24	6^+; 0	88 ± 10		

[a] Primary transition.

[b] Tentative levels observed only in $\gamma_{1\rightarrow 0}$, possibly the known 4^+ at $E_x = 11.93$ MeV and the 6^+ at $E_x = 12.13$ MeV.

[c] Possibly a doublet. See Ref. 28.

^{20}Ne and in the cascade of ^{19}F$(p,\gamma)^{20}$Ne. In addition, there is an established 2^+, ^{20}F state near the corresponding (2.044 MeV) excitation energy.[23] Therefore all evidence supports the existence of a $2^+;1$, ^{20}Ne state at 12.24 MeV.

6. E_a = 9.57 MeV resonance (E_x = 12.39 MeV) (see Fig. 7)

Near 9.57 MeV some weak structure is visible in the RC survey for γ_1, possibly γ_2, and $\gamma_{1\to0}$. The weak nature of this structure, $\omega\gamma_2 = 1.94 \pm 0.15$ eV, coupled with pileup from an intense 6.13 MeV γ ray, inhibited the measurement of the γ_2 primary branch. The 6.13 MeV γ ray results partially from the contaminant reaction ^{13}C$(\alpha,n\gamma)^{16}$O but mainly from the resonance contribution from the inelastic channel ^{16}O$(\alpha,\alpha_2\gamma_{6.13})^{16}$O. Therefore, the angular distribution coefficients and radiative strength were extracted from the NaI yields for γ_1 and the Ge(Li) measured branching ratios were used to calculate the γ_2 strength. Although an isotropic fit to the angular distribution was statistically acceptable, a dipole fit suggests that this decay is either $1^-\to2^+$ or $3^-\to2^+$ ($E1$). A fit to the RC excitation function obtained a resonant energy of 9.57 ± 0.01 MeV and a width of 27 ± 5 keV while a fit to the $\gamma_{6.13}$ resonance (see Fig. 10) obtains $E_R = 9.57 \pm 0.01$ MeV, $\Gamma = 40 \pm 10$ keV.

The global phase shift fit, modified to include ~1% absorption for the inelastic amplitude, determined that $J = 3^-$, $E_R = 9.58 \pm 0.01$ MeV, and $\Gamma = 37 \pm 5$ keV. The γ_2 reduced matrix element, assuming $J = 3^-$, is 1.1×10^{-3} W.u. for an $E1$ decay. While this strength, as discussed in item 3 of this section, may favor a $\Delta T = 1$ transition, it does not exclude $\Delta T = 0$.

Reports on possible ^{20}Ne levels in this region seen through isospin allowed reactions have not always agreed on spin and parity assignments. At present, all evidence (including the RC and ES data of the present work) is consistent with the existence of a 3^- level[5,28,33] near 12.39 MeV and a 0^+ level[5,18,21,42,43] near 12.41 MeV. The 1^+ assignment for the 12.367 ± 0.015 MeV level seen[20] in ^{19}F$(^3$He$,d)^{20}$Ne may have resulted from a failure to resolve this 3^-, 0^+ doublet. The coincidence study ^{19}F$(^3$He$,d\gamma)^{20}$Ne would select only the strongly γ decaying member of the doublet and hence observe[28] only the 3^- state. Although a 0^+ resonance was not included in the ES global phase shift fit near $E_\alpha = 9.6$ MeV, $E_x = 12.41$ MeV [see Fig. 7(b)], the $l = 0$ phase shifts from the second analysis step (where phase shifts were allowed to vary independently with energy) did suggest a 0^+ structure in this region.

The poor fit at $E_\alpha = 9.6$ MeV at angles near P_3 $(\cos\theta) = 0$ [see Fig. 7(b), $\theta = 89°, 104°, 149°$] reflects the need for modified $l = 0$ phase shifts. However since Ref. 42 finds $\Gamma_{\alpha_1}/\Gamma_{\alpha_0} = 6.3$ keV/22.7 keV for the 0^+ state, the competition will damp the ground state resonant behavior.

In ^{20}F there is a 3^- level[34] at 1.97 MeV which might correspond to the 3^-, $E_x(^{20}\text{Ne}) = 12.39$ MeV level. However, there is no known 0^+ corresponding ^{20}F state. Therefore we make a $3^-;(1)$ assignment for the 12.39 MeV state.

7. Other structure

Other possible resonant structures that were observed but not studied in detail will be reported briefly.

Near $E_\alpha = 9.7$ ($E_x = 12.5$) MeV, there may be a weak ($\omega\gamma = 0.17 \pm 0.05$ eV)γ_1 transition, but there is no corresponding strength in $\gamma_{1\to0}$. The investigation of this region was hindered by pileup from the 6.13 MeV γ rays. The ES broad structure was adequately reproduced (see Fig. 8) by a 6^+, $\Gamma = 88$ keV level at 12.59 MeV.

Our phase shift analysis did not require the broad 2^+ level at $E_\alpha = 9.86$ MeV ($E_x = 12.62$) reported by Ref. 5. Some weak, narrow structure is probably present (visible in Fig. 8 only at 67°) near $E_x = 12.49$ MeV but no detailed analysis was performed. This state could correspond to the one reported at $E_x = 12.503 \pm 15$ in the ^{19}F$(^3$He$,d)^{20}$Ne reaction.[20]

Between $E_\alpha = 9.0$ ($E_x = 11.93$) and $E_\alpha = 9.3$ ($E_x = 12.2$) MeV, two resonant structures were located in the $\gamma_{1\to0}$ RC excitation function. We studied this region further since Ref. 4 reported a resonance in the $\gamma_{6.13}$ inelastic channel and there are several ^{20}F states in the corresponding energy region. However, we observed no strong resonances in γ_0 ($\omega\gamma < 0.05$ eV), γ_1 ($\omega\gamma < 0.1$ eV), γ_2 ($\omega\gamma < 0.3$ eV), or $\gamma_{6.13}$ ($\omega\gamma < 10$ eV). Possibly the $\gamma_{1\to0}$ structure may result from a weak γ_2 decays from the 4^+ $E_x = 11.925$ MeV state[35] and the 6^+, $E_x = 12.13$ MeV state.[33] The ES excitation functions were adequately reproduced by a $\Gamma = 30$ keV, 1^- level at $E_\alpha = 9.04$ ($E_x = 11.96$) MeV.

We can compare (see Fig. 11) our observed set of low-lying, natural parity $T = 1$ states with two recent shell model calculations.[36,37] Although we have not located the predicted $0^+;1$ level (the 12.41 MeV level may be a candidate) in the region $10.26 \leq E_x \leq 12.7$ MeV, we have observed the only predicted $1^-;1$ state at 11.26 MeV. Of four predicted $2^+;1$ levels, we have clearly identified only the two at 10.26 and 12.24 MeV. The 11.55 MeV state may also be $2^+;1$ although the corresponding ^{20}F state has not been seen. Two $3^-;1$ levels are predicted, yet only the 12.39 MeV resonance has both 3^- and possible $T = 1$ character. The observed $4^+;1$ state

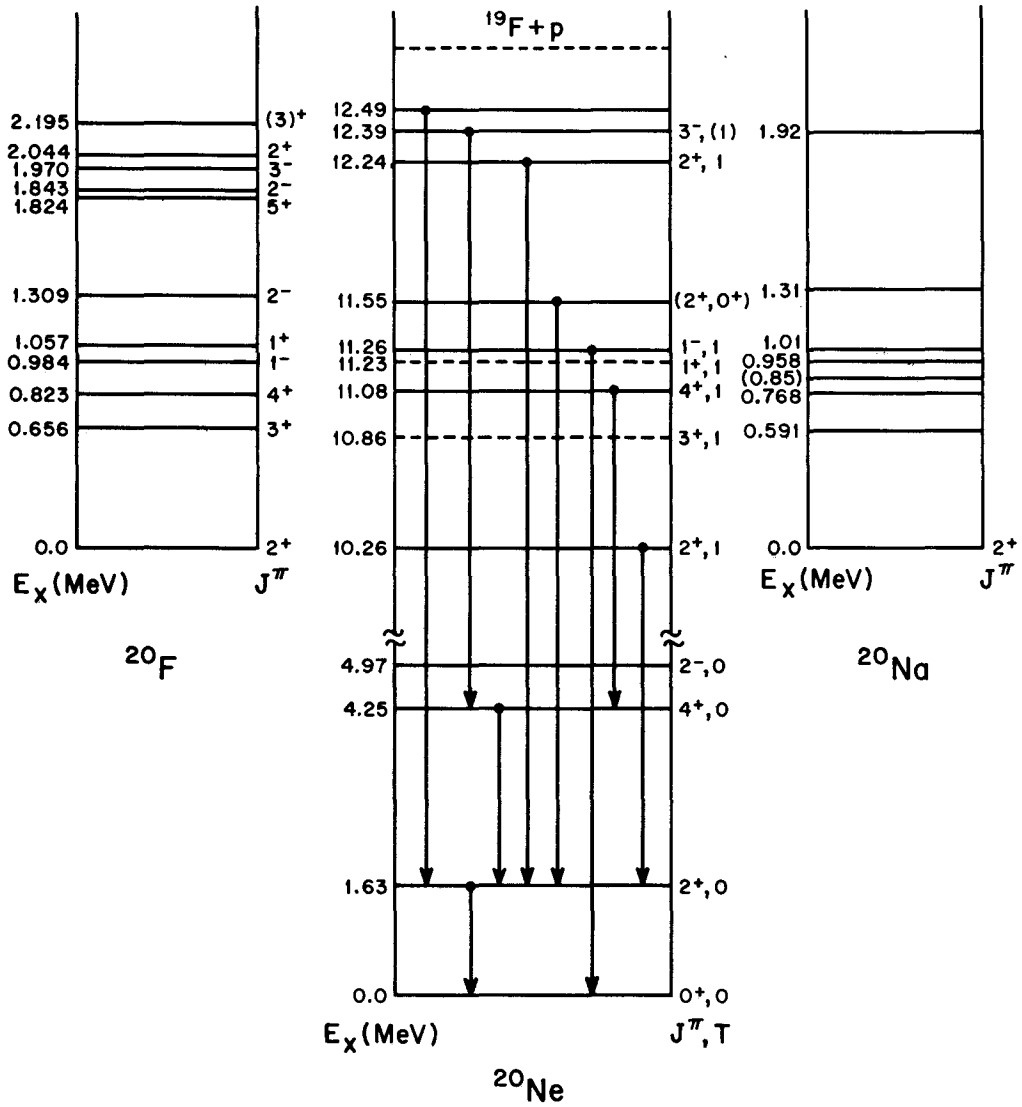

FIG. 11. $A = 20$ levels. An abbreviated ^{20}Ne level diagram shows the primary γ decays observed ($\alpha_2\gamma_{6.13}$ decay of 12.39 MeV state not shown) along with the known ^{20}F and ^{20}Na states. The dashed lines represent unnatural parity, $T = 1$ states not observed in this work. All parameters with the exception of those obtained in this work and some recent assignments in ^{20}F were taken from Ref. 23.

at 11.08 MeV fulfills the prediction of Ref. 36 (Ref. 37 shows another 4^+ at higher energy).

Two recent papers[38,39] provide a simplified framework to analyze the isospin purity of compound nuclear levels with only $T = 0$ particle exit channels. If two levels mix, one primarily $T = 0$ and the other primarily $T = 1$, the isospin purity ($|\epsilon|^2$) can be directly calculated from their observed widths and resonant energies. The charge dependent, mixing matrix element (H_{01}^N) also can be calculated from the experimental resonance parameters. If we knew which $T = 0$ state (antianalog) had a configuration similar to the analog state, we could directly compare our calculated H_{01}^N with a calculated Coulomb mixing matrix element (H_{01}^C) since those two states would mix most strongly. Unfortunately, no theoretical calculations are available for H_{01}^C in ^{20}Ne but calculations[40,41] for nearby nuclei predict $H_{01}^C \approx 20$ to 150 keV. In addition, the identity of the antianalog states has not been established. Although we lack this information, the isospin mixing parameters for $T = 0$ levels near (± 1 MeV) the $T = 1$ levels (see Table VI) can provide some indirect evidence of possible mixing strengths. These results should be interpreted as estimates since (a) only two level mixing has been considered, (b) the $T = 1$ level widths are usually upper limits, and (c) some iso-

TABLE VI. Isospin mixing parameters.

$\|A\rangle$ [a] [E_x (MeV); Γ (keV)]	$\|B\rangle$ (E_x; Γ)	J^π	$\|\epsilon\|^2$ [b]	ϕ_ϵ [b] (rad)	$\|H_{01}^N\|$ (keV)	ϕH_{01}^N (rad)
10.264; 0.13	9.489; 29	2^+	4×10^{-3}	-2×10^{-2}	51 ± 14	-3×10^{-4}
	10.579; 24		5×10^{-3}	4×10^{-2}	23 ± 4	8×10^{-4}
	10.836; 13		1×10^{-2}	1×10^{-2}	56 ± 9	4×10^{-4}
	11.324; 53		2×10^{-3}	2×10^{-2}	52 ± 7	2×10^{-4}
11.077; 0.5 [c]	9.990; 150	4^+	3×10^{-3}	-7×10^{-2}	62 ± 16	-9×10^{-4}
	10.548; 16		3×10^{-2}	-2×10^{-2}	88 ± 22	-2×10^{-3}
	10.790; 350		1×10^{-3}	-5×10^{-1}	13 ± 5	-4×10^{-3}
	11.015; 24		2×10^{-2}	-2×10^{-1}	9 ± 3	-2×10^{-2}
11.259; 0.3 [c]	11.230; 172	1^-	2×10^{-3}	-1.2	4 ± 4	3×10^{-4}
	11.971; 29		1×10^{-2}	2×10^{-2}	71 ± 24	8×10^{-4}
12.237; 18 [c]	11.871; 46	2^+	4×10^{-1}	-9×10^{-2}	119 ± 28	-9×10^{-2}
	12.300; 500		4×10^{-3}	-2×10^{-3}	50 ± 130	-2×10^{-3}

[a] $|A\rangle = \frac{|1\rangle - \epsilon|0\rangle}{(1+|\epsilon|^2)^{1/2}}$, $|B\rangle = \frac{|0\rangle + \epsilon|1\rangle}{(1+|\epsilon|^2)^{1/2}}$.

[b] $|\epsilon|^2 = \Gamma_A/\Gamma_B$, $\tan\phi_\epsilon = (\Gamma_A+\Gamma_B)/2(E_B-E_A)$.

[c] Widths represent estimated upper limits.

[d] Possibly two unresolved narrow levels, see Ref. 28.

spin impurity is present in the incoming channel (^{4}He, 1.3×10^{-5} and ^{16}O, 6.7×10^{-3}). These H_{01}^N estimates are typically of the same order of magnitude as the calculated H_{01}^C for states in nearby nuclei. Therefore if one of the levels near the analog level has a large antianalog component, then it appears likely that the major contribution to H_{01}^N could arise from the Coulomb interaction. However, we cannot draw any more definite conclusions until the structure of these states is established.

VI. CONCLUSIONS

This study of the radiative capture and elastic scattering of α particles by ^{16}O observed six narrow resonant structures that decay to the ground or one of the first two excited states of ^{20}Ne. We establish or confirm J^π for five of these resonances, T for four, and tentatively assign $J^\pi;T$ for the remainder. An improved measurement for $\Gamma_{\gamma1}$ of the 10.264 level brings the radiative transition strength into accord with the analogous β decay measurements and CVC theory. Four of these states are isobaric analog states of ^{20}F. Estimates for the charge dependent matrix elements indicate that if one of the nearby $T=0$ states has significant antianalog character, then one does not need a large charge dependent component in the nuclear interaction to explain these data.

ACKNOWLEDGMENTS

I wish to express my appreciation to Professor H. T. Richards for his interest, guidance, and helpful questioning during this project. I also thank Dr. P. A. Quin and Dr. R. J. Nickles for invaluable discussions on experimental techniques. My appreciation is extended to Dr. H. V. Smith, Dr. L. Chen, Dr. J. Chen, Dr. R. Abegg, J. H. Billen, G. M. Klody, L. C. Boueres, S. Riedhauser, D. Benson, D. Ercegovic, and C. Davis for help in data acquisition. This work supported in part by the U. S. Energy Research and Development Agency.

*Present address: Department of Physics, St. John's University, Collegeville, Minnesota 56321.

[1] D. H. Wilkinson, Phil. Mag. 1, 379 (1956).
[2] W. H. McDonald, Phys. Rev. 101, 271 (1956).
[3] L. C. Chen, Phys. Rev. C 14, 2069 (1976).
[4] J. D. Pearson and R. H. Spear, Nucl. Phys. 54, 434 (1964).
[5] J. John, J. Aldridge, and R. Davis, Phys. Rev. 181, 1455 (1969).
[6] B. Nyman, Nucl. Instrum. Methods 108, 237 (1973).
[7] L. C. Boueres and D. J. Steck, Bull. Am. Phys. Soc. 17, 894 (1972).
[8] D. J. Steck, Ph.D. thesis, University of Wisconsin, 1976 (unpublished). Available through University Microfilms, Ann Arbor, Michigan.
[9] P. Tollefsrud and P. Jolivette, Phys. Rev. C 1, 398 (1970).
[10] B. Singh and H. Evans, Nucl. Instrum. Methods 97, 475 (1971).
[11] E. K. Warburton and J. Weneser, in *Isospin in Nuclear Physics*, edited by D. H. Wilkinson (North-Holland, Amsterdam, 1969), p. 175.

[12]T. Yamazaki, Nucl. Data A 3, 1 (1967).
[13]R. Fletcher and M. Powell, Comput. J. 6, 163 (1963).
[14]H. Seitz, Nucl. Instrum. Methods 86, 157 (1970).
[15]P. Ingalls, Nucl. Phys. A265, 93 (1976).
[16]H. Genz, A. Richter, and B. Schmitz, Nucl. Phys. A267, 13 (1976).
[17]D. Torgerson, K. Wien, Y. Fares, N. Oakey, R. Macfarlane, and W. Lanford, Phys. Rev. C 8, 161 (1973).
[18]B. Lawergren, A. Ferguson, and G. Morrison, Nucl. Phys. A108, 325 (1968).
[19]G. Millington, J. Leslie, W. McLatchie, G. Ball, W. Davies, and J. Forster, Nucl. Phys. A228, 382 (1974).
[20]R. Betts, H. Fortune, and R. Middleton, Phys. Rev. C 11, 19 (1975).
[21]K. Gul, B. Armitage, and B. Hooton, Nucl. Phys. A153, 390 (1970).
[22]D. H. Wilkinson, Phil. Mag. 1, 1031 (1956).
[23]F. Ajzenberg-Selove, Nucl. Phys. A190, 1 (1972).
[24]D. H. Wilkinson, in *Nuclear Spectroscopy*, edited by F. Ajzenberg Selove (Academic, New York, 1960), Pt. B, p. 852.
[25]O. Hausser, T. Alexander, A. McDonald, G. Ewan, and A. Litherland, Nucl. Phys. A168, 17 (1971).
[26]D. Longo, J. Lawson, L. Alexander, B. Hichwa, and P. R. Chagnon, Phys. Rev. C 8, 1347 (1973).
[27]L. Fifield, R. Zurmühle, and D. Balamuth, Phys. Rev. C 14, 1010 (1976).
[28]R. Marrs, E. Adelberger, and K. Snover, Nucl. Phys. A277, 429 (1977).
[29]W. Bendel, L. Fagg, S. Nimrich, E. Jones, and H. Kaiser, Phys. Rev. C 3, 1821 (1971).
[30]K. Hardy and Y. Lee, Phys. Rev. C 7, 1441 (1973).
[31]J. Bishop and H. Fortune, Phys. Rev. Lett. 34, 1350 (1975).
[32]H. Kuan, G. Lutshaw, W. O'Connell, D. Heikkinen, E. Adeleberger, A. Nero, and S. Hanna, Nucl. Phys. A193, 497 (1972).
[33]L. Medsker, H. Fortune, R. Betts, and R. Middleton, Phys. Rev. C 11, 1880 (1975).
[34]H. Fortune and R. Betts, Phys. Rev. C 10, 1292 (1974).
[35]O. Hausser, A. McDonald, I. Szöghy, T. K. Alexander, and D. L. Disdier, Nucl. Phys. A179, 465 (1972).
[36]J. McGrory and B. Wildenthal, Phys. Rev. C 7, 974 (1973).
[37]J. Irvine, G. Mani, V. Pucknell, A. Watt, and R. Whitehead, Phys. Lett. 44B, 16 (1973).
[38]P. E. Shanley, Phys. Rev. Lett. 34, 218 (1975).
[39]C. Waike, Phys. Rev. C 13, 9 (1976).
[40]R. Anderson, M. Wilson, and P. Goldhammer, Phys. Rev. C 6, 136 (1972).
[41]D. Wang and W. Friedman, Phys. Rev. C 12, 1684 (1975).
[42]D. Balamuth, J. Lind, K. Young, Jr., R. Zurmühle, L. Fifield, T. Symons, and K. Allen, Bull. Am. Phys. Soc. 22, 537 (1977); (private communication).
[43]Reported widths and energies differ. Reference 5 claims $\Gamma < 8$ keV, $E_x = 12.41$, while Ref. 42 finds $\Gamma \sim 24$ keV, $E_x = 12.436$. However, for the resonance at $E_x = 11.96$ Ref. 5 claimed $\Gamma = 5.6$ keV whereas the more precise work of Hausser *et al*. Ref. 35 found $\Gamma = 29 \pm 8$ keV in agreement with our value $\Gamma = 30 \pm 5$ keV. We therefore question Ref. 5's value of $\Gamma < 8$ keV.